



UNIVERSITÀ
DEGLI STUDI
FIRENZE

FLORE

Repository istituzionale dell'Università degli Studi
di Firenze

Multiparticle collision simulations of two-dimensional one-component plasmas: Anomalous transport and dimensional crossovers

Questa è la Versione finale referata (Post print/Accepted manuscript) della seguente pubblicazione:

Original Citation:

Multiparticle collision simulations of two-dimensional one-component plasmas: Anomalous transport and dimensional crossovers / Di Cintio, Pierfrancesco; Livi, Roberto; Lepri, Stefano; Ciraolo, Guido. - In: PHYSICAL REVIEW. E. - ISSN 2470-0053. - ELETTRONICO. - 95:(2017), pp. 0-0. [10.1103/PhysRevE.95.043203]

Availability:

This version is available at: 2158/1081246 since: 2017-05-15T16:55:46Z

Published version:

DOI: 10.1103/PhysRevE.95.043203

Terms of use:

Open Access

La pubblicazione è resa disponibile sotto le norme e i termini della licenza di deposito, secondo quanto stabilito dalla Policy per l'accesso aperto dell'Università degli Studi di Firenze (<https://www.sba.unifi.it/upload/policy-oa-2016-1.pdf>)

Publisher copyright claim:

(Article begins on next page)

Multiparticle collision simulations of two-dimensional one-component plasmas: Anomalous transport and dimensional crossovers

Pierfrancesco Di Cintio,^{1,2,3,*} Roberto Livi,^{2,3,4} Stefano Lepri,^{3,4} and Guido Ciriaolo⁵

¹*Consiglio Nazionale delle Ricerche, Istituto di Fisica Applicata “Nello Carrara” via Madonna del piano 10, I-50019 Sesto Fiorentino, Italy*

²*Dipartimento di Fisica e Astronomia and CSDC, Università di Firenze, via G. Sansone 1, I-50019 Sesto Fiorentino, Italy*

³*Istituto Nazionale di Fisica Nucleare, Sezione di Firenze, via G. Sansone 1, I-50019 Sesto Fiorentino, Italy*

⁴*Consiglio Nazionale delle Ricerche, Istituto dei Sistemi Complessi via Madonna del piano 10, I-50019 Sesto Fiorentino, Italy*

⁵*CEA, IRFM, F-13108 Saint-Paul-lez-Durance, France*

(Received 31 October 2016; published 12 April 2017)

By means of hybrid multiparticle collision–particle-in-cell (MPC-PIC) simulations we study the dynamical scaling of energy and density correlations at equilibrium in moderately coupled two-dimensional (2D) and quasi-one-dimensional (1D) plasmas. We find that the predictions of nonlinear fluctuating hydrodynamics for the structure factors of density and energy fluctuations in 1D systems with three global conservation laws hold true also for 2D systems that are more extended along one of the two spatial dimensions. Moreover, from the analysis of the equilibrium energy correlators and density structure factors of both 1D and 2D neutral plasmas, we find that neglecting the contribution of the fluctuations of the vanishing self-consistent electrostatic fields overestimates the interval of frequencies over which the anomalous transport is observed. Such violations of the expected scaling in the currents correlation are found in different regimes, hindering the observation of the asymptotic scaling predicted by the theory.

DOI: [10.1103/PhysRevE.95.043203](https://doi.org/10.1103/PhysRevE.95.043203)

I. INTRODUCTION

Many-particle systems with one or two spatial degrees of freedom d often show anomalous transport properties [1–3]. For nonlinear lattice models, the heat conductivity coefficient κ is found to diverge with the system size N as a power-law for $d = 1$ [4,5], and logarithmically for $d = 2$ [6,7], thus leading to the breakdown of the classical Fourier law. Qualitatively, the anomalous behavior of κ and other transport coefficients can be traced back to the constraints on the dynamics of fluctuations and collective excitations in low dimensionality, as well as to the longer *relaxation times* of the latter. Analytical studies based on nonlinear fluctuating hydrodynamics theory (hereafter NFH) [8–10], unveiled the relation between anomalous transport in anharmonic chains and the fluctuating Burgers–Kardar–Parisi–Zhang (hereafter KPZ) equations for the interface growth [11].

It is nowadays well established on theoretical and numerical grounds that one-dimensional nonlinear systems with three conservation laws (e.g., mass, total energy, and momentum) generically fall in the same KPZ universality class where $\kappa \propto N^{1/3}$ [10,12]. This is somehow intermediate between diffusive ($\kappa \propto N^0$) and ballistic (i.e., $\kappa \propto N$) transport. The latter occurs in integrable models, e.g., the chain of harmonic oscillators [13] and the Toda lattice [14] due to the fact that energy is transmitted through undamped propagation of eigenmodes (respectively, phonons and solitons). More recently, it has been argued that two main nonequilibrium universality classes, the diffusive and KPZ, are only two cases of an infinite discrete family [15]. The members of this family can be identified by their dynamical exponent that depends on

both the number of conserved quantities and on the coupling among their hydrodynamic modes.

If the picture for one-dimensional systems is well developed, much less is known for two-dimensional systems [16,17]. Here a complete NFH theory has not yet been developed and also numerical studies are relatively scarce. For instance, the paradigmatic 2D Ising model shows normal conduction independently on its temperature T [18]. Some numerical studies on 2D square oscillator lattices confirmed the expected logarithmic divergence of heat conductivity [5–7,19]. Evidences of dimensional crossovers from quasi-one-dimensional (1D) to two-dimensional (2D) scaling has been also reported [5,16]. Another remarkable case is the Hamiltonian XY model that displays a transition between logarithmically divergent and normal conductivity when increasing the system temperature T across the Kosterlitz-Thouless-Berezinskii point [20].

This scenario indicates that the problem of heat conduction in 2D systems is far from being completely explored and understood. In this perspective, it is important to investigate how anomalous heat transport changes in the transition between 2D to quasi-1D and 1D systems. Besides this motivation, it is also relevant to go beyond lattice models to assess the universality hypothesis in the more general contest of classical and quantum fluids and even plasmas in low-dimensions.

In this paper we aim at exploring the above questions in the context of a simple model for a 2D plasma and to study its statistical properties as measured by the correlation functions of the fluctuations of the conserved fields. In particular, we will focus on a *one-component plasma* (OCP) [21,22]. Such a model, despite its highly idealized nature, is suitable to treat a broad range of plasma regimes. For instance, OCP models have been applied to the study of relaxation in ultracold plasmas [23,24], phase transitions in Coulomb crystals [25–27], neutron-star crust crystallization

*p.dicintio@ifac.cnr.it

[28–30], cooling of magnetized plasmas [31,32], degenerate inertial-fusion plasmas [33], as well as charged colloids in solution [34,35] and Yukawa liquids [36,37]. For an extensive review see Ref. [38] and references therein.

The simulation studies are carried using the multiparticle collision algorithm (MPC) first introduced by Malevanets and Kapral [39,40] and later widely employed for the simulation of the mesoscopic dynamics of polymers in solution, colloidal fluids, and other complex fluids (e.g., see Ref. [41] and references therein). Such method is based on a mesh-dependent stochastic rule mixing particle velocities, constrained by the local conservation of kinetic energy, momentum, and angular momentum. Application of the technique in plasma physics is, at the best of our knowledge, new [42] and has its own interest as a promising tool to investigate a variety of problems, such as, for example, transport in complex magnetized plasmas [32,43], discreteness effects in charged particle beams dynamics [44,45], as well as collision-driven transport of neutrals in fusion plasmas [46,47].

The paper is structured as follows: in Sec. II we introduce the model and the main quantities of interests, in Sec. III we detail the numerical code (multiparticle collision) used for the simulations, in Sec. IV we show the results for 2D systems and quasi-1D systems, with respect also to our previous results on the 1D version of the model, as well as the effect of a self-consistent electrostatic field. Finally, in Sec. V we summarize and point out the possible development of this work. The Appendix contains some details on the implementation of conservation laws in the numerical code employed in this paper.

II. THE MODEL

We consider a OCP, namely a system of N_p charged particles of charge q and mass m (e.g., electrons), embedded in a neutralizing and static homogeneous background (e.g., ions) with charge density ρ . The state of a OCP is fully determined by a single macroscopic quantity, the plasma coupling parameter, usually defined [38,48] as the ratio of a typical nearest-neighbor interaction potential energy and mean thermal energy as

$$\Gamma \equiv \frac{\bar{U}}{k_B T}. \quad (1)$$

In the equation above, k_B and T are the Boltzmann constant and the plasma temperature (or the average particle kinetic energy $\langle K \rangle$ if the system is not in thermal equilibrium), respectively, while the form of the mean interparticle Coulomb potential energy \bar{U} depends on the dimensionality of the system and the screening of counter-charges [49]. Typically, it is assumed that

$$\bar{U} = \frac{q^2}{4\pi\epsilon_0 a}, \quad (2)$$

where ϵ_0 is the permittivity of free space, and the Wigner-Seitz radius a defines the average interparticle distance as function of the number density n as $(4\pi n/3)^{-1/3}$ in 3D, and $(2\pi n)^{-1/2}$ in 2D [36].

Hereby we consider a 2D globally homogeneous neutral OCP, for which the typical interaction range is given by the

2D Debye length,

$$\lambda_D = \sqrt{\epsilon_0 k_B T a / q^2 n}. \quad (3)$$

It remains to introduce at this point the two principal time scales of the system, t_{dyn} and t_{coll} , associated to the collective modes (e.g., the so-called Langmuir waves [50]), and to the collisionality of the system, respectively. In a 2D OCP the dynamical time t_{dyn} is related to the 2D plasma frequency Ω_P [36,51] by

$$t_{\text{dyn}} = 4\pi / \Omega_P, \quad \Omega_P = \sqrt{nq^2 / 2\epsilon_0 a m}, \quad (4)$$

while the collision time t_{coll} is the inverse of the collision frequency [52] and reads,

$$t_{\text{coll}} = 1 / \Omega_{\text{coll}}, \quad \Omega_{\text{coll}} = \frac{nq^4 \ln \Lambda}{2\pi a \epsilon_0^2 m^{1/2} (k_B T)^{3/2}}. \quad (5)$$

The expression for Ω_{coll} has been rescaled ad hoc in order to account for the fact that the system is defined in 2D and n has the meaning of a surface number density. In the equation above, the argument of the Coulomb logarithm $\ln \Lambda$ is somewhat arbitrary, we take here $\Lambda = \lambda_D / a_{\text{min}}$, where the typical minimum inter-particle distance is usually $a_{\text{min}} \approx a / 10$ for our choice of parameters.

As we are primarily interested in the collision-driven energy transport, throughout this work we will consider only nondegenerate regimes for which $a < \lambda_D$, excluding, for example, ultra correlated plasmas (i.e., $\Gamma > 200$) for which a exceeds λ_D , as well as extremely collisionless systems where $t_{\text{coll}} \gg t_{\text{dyn}}$ ($\Omega_{\text{coll}} \ll \Omega_P$).

In order to study the transport properties of the OCP, we measure the thermal conductivity κ making use of the Green-Kubo formula,

$$\kappa = \frac{D}{k_B T^2 N} \int_0^\infty \langle \mathbf{J}_E(t) \mathbf{J}_E(0) \rangle_{\text{eq}} dt, \quad (6)$$

where D is a dimensional constant and $\langle \mathbf{J}_E(t) \mathbf{J}_E(0) \rangle_{\text{eq}}$ is the equilibrium time-correlation function of the energy current,

$$\mathbf{J}_E(t) = \sum_{j=1}^{N_p} \mathcal{E}_j \mathbf{v}_j. \quad (7)$$

For charged systems the particle energy \mathcal{E}_j is given by

$$\mathcal{E}_j = \frac{m \mathbf{v}_j^2}{2} + q \Phi(\mathbf{r}_j), \quad (8)$$

wherein $\Phi(\mathbf{r})$ is the electrostatic potential due to the charge distribution and/or, eventually, an external contribution. In the formulas above, \mathbf{r}_j and \mathbf{v}_j are particles positions and velocities.

In 1D systems, where typically $\kappa \propto N^\gamma$, an effective way for obtaining the exponent γ amounts to estimate the low frequency behavior of [1,2]

$$C_E(\omega) = \langle |\hat{\mathbf{J}}_E(\omega)|^2 \rangle \sim \omega^{-\gamma}, \quad \text{for } \omega \rightarrow 0, \quad (9)$$

i.e., the Fourier transform of $\langle \mathbf{J}_E(t) \mathbf{J}_E(0) \rangle_{\text{eq}}$.

For 2D systems, instead, the logarithmic divergence of κ with the size N amounts to a t^{-1} decay of the correlations, which is equivalent to

$$C_E(\omega) \sim [\alpha - \beta \log(\omega)], \quad \text{for } \omega \rightarrow 0, \quad (10)$$

where α and β are two positive constants (see, e.g., Ref. [20], and references therein).

In order to provide a complete description of the transport process of the model we analyze also the charge density current correlator $C_\rho(\omega)$, defined in the same fashion as $C_{\mathcal{E}}(\omega)$. The spatial density of a system of discrete charges q in a homogeneous neutralizing background ϱ is defined as

$$\rho(\mathbf{r}) = \varrho + \sum_{j=1}^{N_p} [q\delta(\mathbf{r} - \mathbf{r}_j)], \quad (11)$$

so that the charge current \mathbf{J}_ρ reads

$$\mathbf{J}_\rho(t) = \sum_{j=1}^{N_p} [\varrho + q\delta(\mathbf{r} - \mathbf{r}_j)]\mathbf{v}_j. \quad (12)$$

As we are going to discuss in Sec. IV, a special importance for our analysis is played also by the density dynamical structure factor $S_\rho(\mathbf{k}, \omega)$, containing information on the inter-particle correlations and their time evolution. This quantity is constructed in our numerical simulations as follows: first of all, we introduce the spatial Fourier transform of the density at a given time t , which reads according to the definition of $\rho(\mathbf{r})$ given in Eq. (11) (see also [53]), as

$$\hat{\rho}(\mathbf{k}, t) = \varrho\delta(\mathbf{k}) + \frac{1}{N_p} \sum_{j=1}^{N_p} q \exp[i2\pi\mathbf{k} \cdot \mathbf{r}_j(t)], \quad (13)$$

where the first term arises from the definition of Fourier transform of a constant. We then take the temporal discrete Fourier transform of $\hat{\rho}(\mathbf{k}, t)$ at fixed wave number \mathbf{k} that yields

$$\begin{aligned} \hat{\rho}(\mathbf{k}, \omega) &= \frac{1}{N_t} \sum_{l=1}^{N_t} \hat{\rho}(\mathbf{k}, t_l) \\ &\times \left[\cos\left(-\frac{2\pi t_l \omega}{N_t}\right) + i \sin\left(-\frac{2\pi t_l \omega}{N_t}\right) \right], \end{aligned} \quad (14)$$

where N_t is the total number of equally sized time steps Δt performed by the simulation, so that $t_l = l \Delta t$. Finally, by taking the modulus square of $\hat{\rho}(\mathbf{k}, \omega)$, we obtain

$$S_\rho(\mathbf{k}, \omega) = \langle |\hat{\rho}(\mathbf{k}, \omega)|^2 \rangle_{\text{eq}}. \quad (15)$$

Note that, in our numerical implementation, the temporal Fourier transform of charge density appearing in Eq. (14) is computed only for a small number of wave vectors \mathbf{k} , thus avoiding to increase dramatically the memory load. On the other hand, we are primarily interested to analyze the hydrodynamic limit of the model, which corresponds to consider only low- \mathbf{k} modes. Note also that, instead of evaluating $\hat{\rho}(\mathbf{k}, t)$ as in Eq. (11), one could in principle coarse grain the density on a mesh [cf. Eq. (26) in the following section] and then take its time transform.

III. THE NUMERICAL CODE

At variance with the pioneering numerical studies on the OCP based on direct molecular dynamics [54–56], and more recent numerical work involving particle-particle-particle

mesh codes (P³M; see Ref. [57]) [36,58], in this work we adopt a novel computational approach, effectively splitting the Coulomb interaction in its short- and long-range contributions, treating them with a hybrid multiparticle-collision (MPC)–particle-in-cell (PIC) code.

As in standard mesh-based computational schemes, the spatial domain of the simulation is coarse-grained into equal cells of size Δs . Inside each cell, Coulomb scatterings among particles are resolved *stochastically* by mixing in a collision step the particles velocities, so that their total momentum, kinetic energy, and angular momentum are conserved; while during the “streaming” step, the same are updated along with the associated position under the effect of the self-consistent electromagnetic field, computed on the grid with the usual PIC or particle-mesh technique [59].

A. The multiparticle collision scheme

The MPC codes nowadays used in numerical complex fluid dynamics rely on different velocity exchange rules (see, e.g., Ref. [60] for an extensive review). Here, we briefly review the general implementation of the widely used *stochastic rotation dynamics* (hereafter SRD).

Let us consider a system of N_p equal particles partitioned into N_c equal volume cells in Cartesian coordinates. The particles move in continuum 2D space with momentum $\mathbf{p}_j = m\mathbf{v}_j$, either freely or under the effect of an external and/or self-consistent force field. In order to perform a collision step in the i th cell one has to compute first its center of mass velocity,

$$\mathbf{u}_i = \frac{1}{M_i} \sum_{j=1}^{N_i} \mathbf{p}_j, \quad M_i = \sum_{j=1}^{N_i} m = mN_i, \quad (16)$$

where N_i is the number of particles in the cell. The collision amounts to a rotation $\hat{\mathbf{R}}$ of an angle $\pm\varphi_i$ with probability one-half of the *relative* velocities $\delta\mathbf{v}_j = \mathbf{v}_j - \mathbf{u}_i$, namely

$$\mathbf{v}'_j = \mathbf{u}_i + \hat{\mathbf{R}}_i \cdot \delta\mathbf{v}_j. \quad (17)$$

Such a rotation guarantees the conservation of the total momentum and kinetic energy in the cell:

$$\mathbf{P}_i = \sum_{j=1}^{N_i} m\mathbf{v}_j = \sum_{j=1}^{N_i} m\mathbf{v}'_j, \quad (18)$$

and

$$K_i = \frac{1}{2} \sum_{j=1}^{N_i} m\mathbf{v}_j^2 = \frac{1}{2} \sum_{j=1}^{N_i} m\mathbf{v}'_j{}^2. \quad (19)$$

However, with such a choice of the velocity rotation protocol, the total angular momentum L_i in the cell is not conserved [61].

Several MPC algorithms that account for the angular momentum conservation do exist [61–63]. In this paper we impose also this conservation law by adopting the so-called deterministic rotation scheme (DR, originally introduced in Ref. [64]; see also Refs. [60,62]) that applies only to 2D systems. In practice, the cell-dependent rotation angle φ_i that defines $\hat{\mathbf{R}}_i$ in Eq. (17) is evaluated deterministically from the

relation

$$\sin \varphi_i = -\frac{2a_i b_i}{a_i^2 + b_i^2}, \quad \cos \varphi_i = \frac{a_i^2 - b_i^2}{a_i^2 + b_i^2}, \quad (20)$$

where the coefficients a_i and b_i are given as functions of particles' positions and velocities by

$$a_i = \sum_{j=1}^{N_i} \mathbf{r}_j \wedge (\mathbf{v}_j - \mathbf{u}_i), \quad (21)$$

and

$$b_i = \sum_{j=1}^{N_i} \mathbf{r}_j \cdot (\mathbf{v}_j - \mathbf{u}_i), \quad (22)$$

where \wedge denotes the external product in two dimensions. With such a choice of φ_i the angular momentum conservation in cell i reads

$$L_i = \sum_{j=1}^{N_i} m(\mathbf{r}_j \wedge \mathbf{v}_j) = \sum_{j=1}^{N_i} m(\mathbf{r}_j \wedge \mathbf{v}'_j). \quad (23)$$

The proof of the angular momentum conservation under a DR move is reported in the Appendix, along with the proof of kinetic energy and linear momentum under the more general SRD scheme.

Note that, since we are considering point-like particles, the contribution of an internal degree of freedom associated to particle size (i.e., a classical spin) does not enter the definition of L and its local conservation under MPC dynamics. However, due to the imposed *periodic* boundary conditions (PBC) in our simulation setup, L is not globally conserved. In practice, the angular momentum l_i of a particle i of mass m with velocity $\mathbf{v}_i = (v_{xi}; v_{yi})$ changes as the latter crosses an edge of the simulation domain (e.g., $x_{\max}; y$), and it is reinjected at the opposite one ($x_{\min}; y$); i.e.,

$$l_i = m(x_{\max} v_{yi} - y_i v_{xi}) \neq m(x_{\min} v_{yi} - y_i v_{xi}). \quad (24)$$

It is important to remark at this stage, that in order to correctly reproduce the hydrodynamics of the system, the conservation rules should indeed be *local* (i.e., at the cell level in our case), as proved in Ref. [65], and therefore the violation of the global conservation of L_{tot} due to the choice of PBC is irrelevant. In fact, in our simulations we always start with null total angular momentum and the fluctuations due to the boundary effect average to zero.

Moreover, note also that, with the implementations of the MPC method described here, the Galilean invariance of the particle equations of motion is violated. To avoid this complication, before the collision step all particles of the simulation are shifted by the same vector \mathbf{d} with components d_x, d_y , chosen from a uniform distribution between $\Delta s/2$ and $-\Delta s/2$, where Δs is the cell size. After the collision, the particles are shifted back of $-\mathbf{d}$ to their original position. It has been proved, that if the system mean path $\lambda_{\text{coll}} > \Delta s/2$, the violation of the Galilean invariance is negligible [66,67].

Up to now, we reviewed the SRD and DR in the standard fluid case. In a series of papers on the anomalous diffusion and heat transfer in 1D one-component plasmas [42,68,69], we have adapted a reduced version of the MPC technique

to treat a fluid of particles interacting via effective Coulomb forces, by conditioning the velocity exchange to an interaction probability \mathcal{P}_i , which depends on the values of the plasma parameters in the cell.

In this work, we proceed in the same fashion introducing for each cell the *local* plasma coupling parameter [cf. Eqs. (1) and (2)], $\bar{\Gamma}_i = \bar{U}_i / \bar{K}_i$, where \bar{U}_i and $\bar{K}_i = K_i / N_i$ are the mean interparticle potential energy and mean kinetic energy in cell i , respectively. In order to account for the logarithmic nature of the Coulomb interaction in two dimensions [70], \bar{U}_i is corrected by the multiplicative factor $-\log(a_i / \Delta s)$, where $a_i = (N_i / \Delta s^2)^{-1/2}$. Note that, in the range of parameters considered here, such quantity is always positive and of order 1.

During the collision step, the multiparticle collision probability is evaluated as

$$\mathcal{P}_i = \frac{1}{1 + \bar{\Gamma}_i^{-2}}. \quad (25)$$

By sampling a random number \mathcal{P}_i^* from a uniform distribution in the interval $[0, 1]$, the rotation (i.e., the multiparticle collision) Eq. (17) runs if $\mathcal{P}_i^* / \mathcal{P}_i \leq 1$.

Note that the formulas above are written for a single-mass system. However, several generalizations of the MPC technique to the case of multimass systems do exist (see, e.g., Ref. [41]). Hereafter, we will only deal with single species systems, where all $m_j = m$.

From a practical point of view this probabilistic interaction rule, inspired by heuristic arguments, is equivalent to adopt a distribution of the time between collision events in each cell. Translation invariance guarantees that this distribution is independent of cell i . We have also checked that in a wide range of parameters this distribution is Poisson-like and its typical time scale depends on Γ .

B. Computation of the self-consistent electrostatic field and tests

In order to obtain a more complete picture of the transport properties of the system, we also study the contribution of its self-consistent electrostatic field \mathbf{E} , evaluated with the standard particle-mesh technique with a Fourier space-based Poisson-solver [59]. In the numerical calculations presented in this paper, we consider 2D systems in a rectangular simulation box with periodic boundary conditions, partitioned in $N_c = N_x \times N_y$ equal square cells of size Δs . In each cell the charge density $\rho_{i,j}$ is given by

$$\rho_{i,j} = q_{i,j} + \frac{1}{\Delta s^2} \sum_{k=1}^{N_{i,j}} q_k, \quad (26)$$

where $N_{i,j}$ is the number of particles in the cell while q_k are their charges. For the sake of simplicity we assume that the fixed neutralizing background density is everywhere constant, i.e., $q_{i,j} = \varrho$. In practice, the electrostatic field can be evaluated by the standard equation $\mathbf{E}(\mathbf{r}) = -\nabla \Phi(\mathbf{r})$, where the electrostatic potential $\Phi(\mathbf{r})$ is related to the charge density by the Poisson equation $\Delta \Phi(\mathbf{r}) = \rho(\mathbf{r}) / \epsilon_0$, which is easier to be solved in Fourier space; see, e.g., Ref. [71], and references therein.

In our code, the Fourier transforms are computed with the publicly available FFTW package [72]. Eventually, when $\Phi(\mathbf{r})$ is obtained the electric field is evaluated at each particle position by standard two-dimensional interpolation procedures [73].

The particles equations of motion under the effect of the electric field \mathbf{E} are integrated in our FORTRAN90 code (see also Ref. [74] for further details), with the standard second order *leapfrog* scheme, widely used in molecular dynamics simulations [75,76]. For all simulations presented here we use a *bona fide* fixed timestep $\Delta t = 0.05t_{\text{dyn}}$ ensuring energy conservation up to 1 part in 10^{-12} when using double precision, while still allowing for acceptable computational times on a single core of an i5 HP machine running LINUX.

In the present paper we investigate only periodic systems with global charge neutrality, characterized by *equilibrium* phase-space distribution function,

$$f(\mathbf{r}, \mathbf{v}) = \frac{Cn}{2\pi m k_B T} \exp(-m\mathbf{v}^2/2k_B T), \quad (27)$$

where n is the (spatially constant) number density and C is a normalization factor so that the integral of f over the simulation domain equals 1.

Note that for this class of initial conditions, the average self-consistent electrostatic field is zero, because the counter background charge screens the long-range tail of the Coulomb interaction. However, spatiotemporal fluctuations of the field $\mathbf{E}(\mathbf{r}_i)$ persist. We performed test simulations of globally neutral equilibrium systems for different values n and different combinations of system size and grid resolution. We found that, for $N_c = N_x \times N_y \geq 50$, the electrostatic field averaged over the particle positions is actually zero, independently on the systems size. For fixed n and fixed cell size Δs , the amplitude of its fluctuations $\sigma_{\mathbf{E}}$ decrease with the systems size as a power-law as shown in Fig. 1 for the x component of \mathbf{E} .

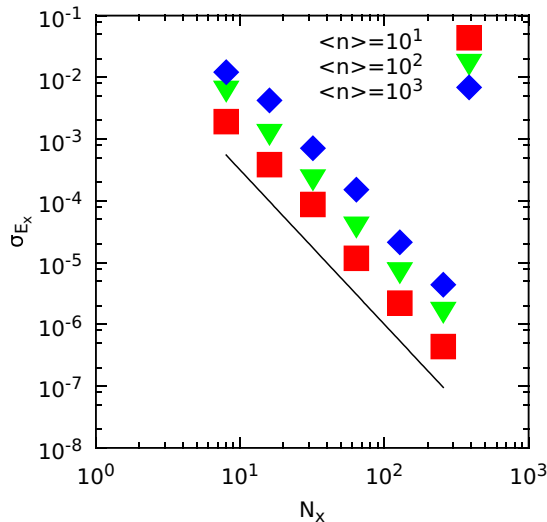


FIG. 1. Fluctuations σ_{E_x} of the x component of the electrostatic field as function of the cell number N_x along x , for different values of the particle number density n . The solid line marks the fitting power-law trend obtained by the data points $\sigma_{E_x} \propto N_x^{5/2}$.

In this paper, we want also to address the question if the presence of such fluctuations of \mathbf{E} have an influence on the hydrodynamic behavior of 2D neutral plasmas. In the following section, we report two sets of numerical experiments for fixed plasma parameters. In the first case we impose $\Phi = 0$, so that the conserved total energy is reduced to the kinetic term only, and particles move freely between collisions. In the second case Φ is computed from the instantaneous distribution of particles whose dynamics depends also on the fluctuating field \mathbf{E} . Despite the amplitude of fluctuations in the explored regimes is quite small, the presence of the fluctuating field could yield some changes in the hydrodynamic behavior of the system. In fact, as discussed in the following section, it does not affect significantly the form of the structure factors, but, this notwithstanding, the low-frequency component of the energy current frequency spectrum exhibits some difference, that can be attributed to finite-size effects.

In the present work we do not investigate regimes where the self-consistent electric field is large, as it happens for sensible charge unbalance or in the presence of an external potential. These cases will be analyzed in a forthcoming publication.

All numerical simulations presented in this paper have been carried out making use of units such that $k_B = \epsilon_0 = m = q^2 = 1$, while the normalization of distances is fixed so that the cell length $\Delta s = \lambda_D = 1$. With such a choice, the numerical model has only two control parameters, i.e., the temperature T and the average number density n that combined together yield Γ .

IV. RESULTS

A. Two-dimensional systems

In a first set of numerical simulations we study the behavior of the energy and density correlators of 2D OCP for different systems sizes and values of Γ . The initial conditions are generated by sampling particles positions and velocities from the phase-space distribution Eq. (27) for the chosen values of temperature T and particle density n .

The particles equations of motion have been integrated over a time scale $t_{\text{end}} \approx 7000t_{\text{dyn}}$. Such a choice guarantees a good convergence to equilibrium over the explored range of parameters.

The main result of our study is that the correlator of the energy current $C_{\mathcal{E}}(\omega)$ always shows a clear logarithmic behavior for low ω , as expected on the basis of general theoretical arguments (see, e.g., Ref. [1]).

In Fig. 2 we show $C_{\mathcal{E}}(\omega)$ for an OCP with $\Gamma = 3$, for different system sizes ranging from $N_c = 8^2$ up to 256^2 . All curves appear to be well fitted by Eq. (10) in the interval of frequencies $10^{-2} \leq \omega/\Omega_p \leq 10$.

The robustness of this logarithmic scaling can be tested while varying Γ (e.g., varying T at fixed n or, viceversa fixing T and varying n). In Fig. 3 we report the normalized quantity $C_{\mathcal{E}}(\omega)/C_{\mathcal{E}}(\Omega_p)$ versus ω/Ω_p for fixed system size (in units of its λ_D) while varying Γ over five orders of magnitude. We find that the logarithmic fit is maintained and is optimal for $\Gamma \approx 1$, which is at the border between strong and weak coupling regimes. In addition, we have also checked that simulations with initial conditions characterized by different combinations

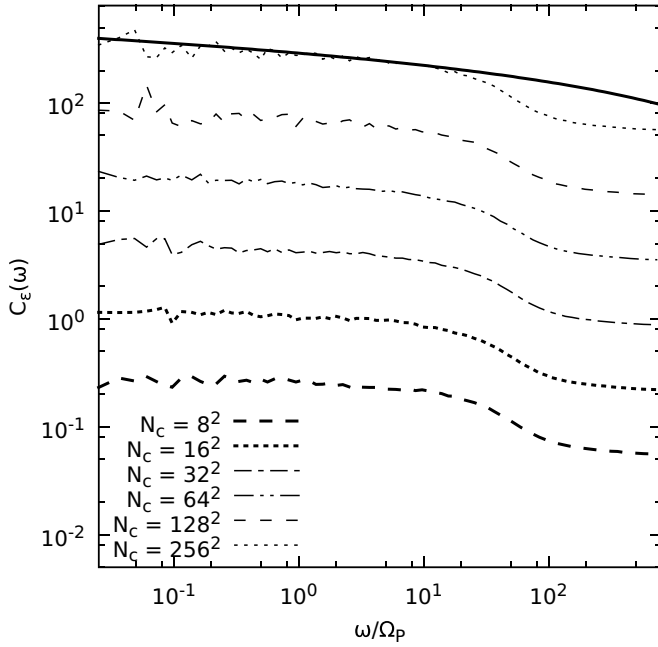


FIG. 2. Fourier spectra C_E of the energy current, for $\Gamma = 3$, and $N_c = 8^2, 16^2, 32^2, 64^2, 128^2$, and 256^2 (dashed lines). To guide the eye, the fitting function $f(\omega) \propto \alpha - \beta \log(\omega)$ is added to the figure (heavy solid line).

of T and n yielding the same values of Γ are associated with qualitatively similar results.

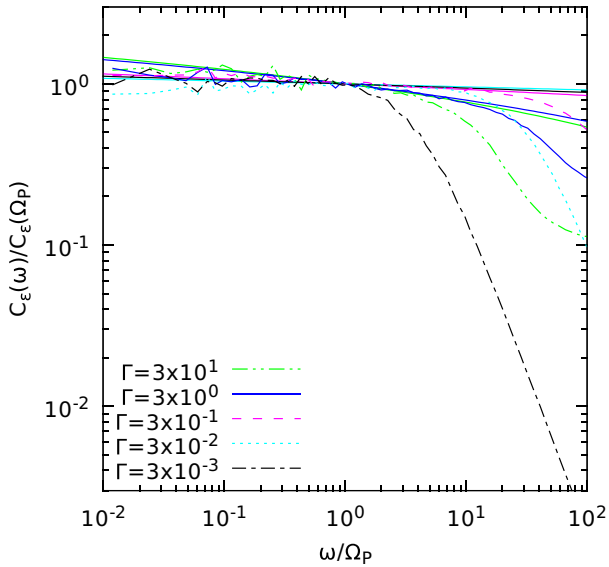


FIG. 3. Normalized Fourier spectra of the energy current C_E for 2D systems with different values of the plasma coupling parameter $10^{-3} < \Gamma < 10^2$ (dashed lines). The frequency is in units of Ω_p as given in Eq. (4), while the correlator scale is in units of the corresponding $C_E(\Omega_p)$. For each case, the best-fit curve according to Eq. (10) is added (solid lines).

B. Dimensional crossover

In the previous section we have checked the expected logarithmic divergence Eq. (10) of the energy current correlator of the 2D OCP model. Here we investigate how such a behavior crosses over to the power-law behavior predicted by the KPZ hydrodynamics when passing from 2D to quasi-1D systems.

In the simulations reported hereafter we fix $\Gamma = 3$ (i.e., moderately coupled particles) and $N_x = 256$, while $2 \leq N_y \leq 256$ (i.e., $1/128 \leq L_y/L_x \leq 1$). Notice that for the adopted value of Γ , $\Omega_{\text{coll}} > \Omega_p$, so that the contribution of the fluctuating electrostatic field on the collisional dynamics is very small. For the sake of simplicity in these simulations we have set $\mathbf{E} = 0$. In the following subsection we shall analyze also the effects of a nonzero electrostatic field.

In Fig. 4 we show the Fourier spectra of the energy and density current correlators $C_E(\omega)$ [Fig. 4(a)] and $C_\rho(\omega)$ [Fig. 4(b)] for different values of N_y . For small values of N_y

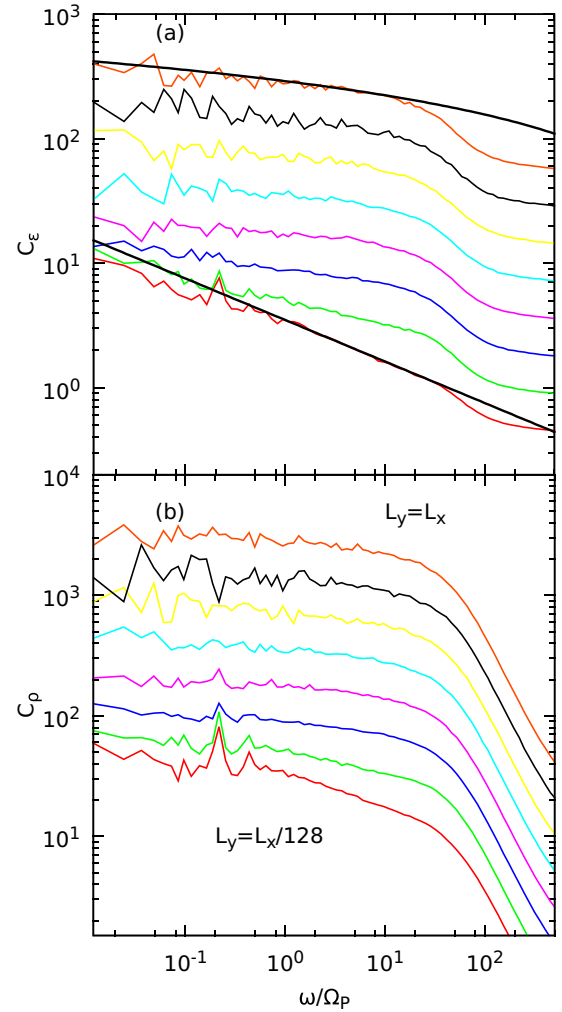


FIG. 4. Fourier spectra of the energy current C_E , panel (a) and of the density current C_ρ , panel (b) as function of the frequency ω normalized to Ω_p , for $\Gamma = 3$, and $L_x/L_y = 128, 64, 32, 16, 8, 4, 2$, and 1 . The curves are averaged over 100 independent realizations. The two heavy solid lines in panel (a) mark the predicted $\omega^{-1/3}$ and $\alpha - \beta \log \omega$ trends in pure 1D and 2D cases, respectively.

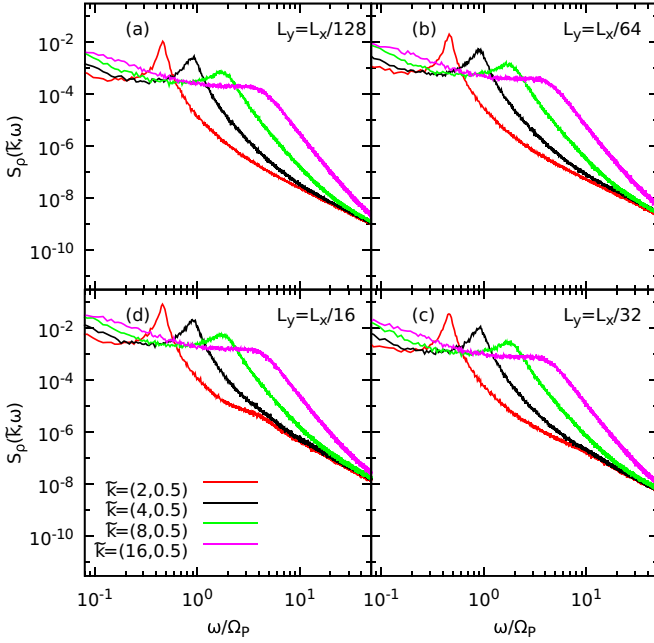


FIG. 5. Dynamical structure factor of density S_ρ for $\tilde{\mathbf{k}} = (2, 0.5)$, $(4, 0.5)$, $(8, 0.5)$, and $(16, 0.5)$, $N_x = 256$ and $N_y = 2$ (a), 4 (b), 8 (c), and 16 (d). In all cases $\Gamma = 3$.

$C_{\mathcal{E}}(\omega)$ exhibits a $\omega^{-1/3}$ slope for small values of ω , typical of 1D systems with three conservation laws, while the logarithmic singular behavior is recovered for sufficiently large value of N_y . In particular, the crossover between these different scaling laws can be approximately identified for $N_y = 8$ (i.e., $L_y = L_x/16$, see the third curve from below).

For what concerns $C_\rho(\omega)$ for small values of N_y we recover the same power-law behavior observed in Ref. [42] for a 1D OCP. When N_y is increased the exponent of the power law seems just to decrease. We conjecture that a logarithmic singularity could be recovered also for $C_\rho(\omega)$ by simulating much larger systems, a check that is far beyond our computational resources.

Moreover, we have also computed the density structure factor $S_\rho(\mathbf{k}, \omega)$, that has been used as a testbed to check the validity of KPZ fluctuating hydrodynamics in 1D OCP (see Figs. 6 and 7 in Ref. [42]).

In Fig. 5 we show $S_\rho(\tilde{\mathbf{k}}, \omega)$ for N_y significantly smaller than $N_x = 256$. For each value of N_y we report the data corresponding to four low values of the normalized wave number $\tilde{\mathbf{k}} = (2, 0.5)$, $(4, 0.5)$, $(8, 0.5)$, and $(16, 0.5)$, that point out the hydrodynamic limit of the model. As already observed for 1D models (cf. Figs. 1 and 6 in Ref. [42]), also these curves exhibit a peak at $\omega_{\max} \propto c_s \|\mathbf{k}\|$ (c_s is the sound velocity of the system) that sharpens for decreasing values of \tilde{k} and L_y .

The prediction of the NFH theory [9] for 1D systems is that the density correlation in the large-time and space scales should obey the dynamical scaling of the KPZ equation. Accordingly, the structure factor $S(k, \omega)$ for small enough wave numbers k and $\omega \approx \pm\omega_{\max}$, are expected to scale as

$$S_\rho(k, \omega) \sim h_{\text{KPZ}} \left(\frac{\omega - \omega_{\max}}{\lambda_s k^{3/2}} \right), \quad (28)$$

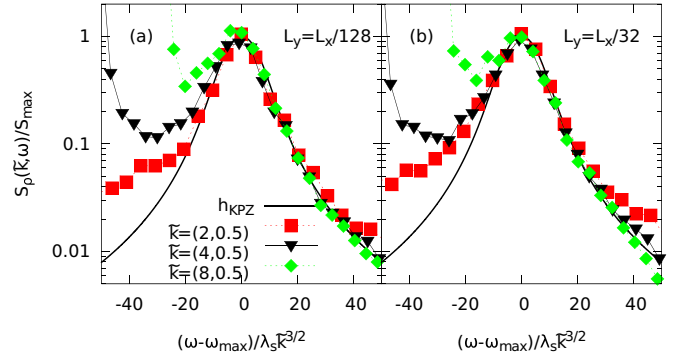


FIG. 6. Data collapse of the rescaled structure factor (points) to the KPZ scaling function h_{KPZ} (solid lines) for the modes corresponding to $\tilde{\mathbf{k}} = (2, 0.5)$ (squares), $(4, 0.5)$ (downward triangles), and $(8, 0.5)$ (diamonds). Panel (a) refers to $N_y = 2$ (i.e., $L_y = L_x/128$), and the panel (b) to $N_y = 8$ (i.e., $L_y = L_x/32$).

where λ_s is a model-dependent coefficient that can be evaluated in terms of equilibrium correlators, and h_{KPZ} is the universal KPZ scaling function that is not known in terms of simple functions [9]. Asymptotic and integral forms of Eq. (28) are given, e.g., in Ref. [77].

It becomes natural to ask whether (and to which extent) the peaks of $S_\rho(\tilde{\mathbf{k}}, \omega)$ are fitted by the KPZ scaling function. In order to test the quality of the fit, we have rescaled the longitudinal component of $S_\rho(\tilde{\mathbf{k}}, \omega)$ according to Eq. (28), for the cases presented in Fig. 5. In Fig. 6 we show that the structure factors obtained for $N_y = 2$ and 8 exhibit a good data collapse onto the KPZ scaling function for $\tilde{\mathbf{k}} = (2, 0.5)$, $(4, 0.5)$, and $(8, 0.5)$. This analysis indicates that the system maintains the same hydrodynamic features of a genuine 1D system. Moreover, also in the cases reported in Fig. 6, the data collapse is very poor for larger values of $\tilde{\mathbf{k}}$ (data not shown), because of the presence of the heat mode peak at low values of ω [53].

Conversely, we expect that approaching the 2D limit $N_y \sim N_x$ the data collapse on the KPZ scaling function will not hold for small values of $\tilde{\mathbf{k}}$. As shown in Fig. 7 for $N_y = 64$ we still obtain for $\tilde{\mathbf{k}} = (2, 0.5)$, $(4, 0.5)$, and $(8, 0.5)$ a good data collapse of the structure factors, which can be fitted empirically by a rational function,

$$S_\rho(k, \omega) \sim h_{2\text{D}} \equiv C \left[\left(\frac{\omega - \omega_{\max}}{H_k} \right)^\xi + 1 \right]^{-\zeta}, \quad (29)$$

where H_k is the full-width-at-half-maximum of the sound peak, C is scale factor depending on the normalization choice of ω , and the numerical estimates of the exponents yield $\xi \approx 2$ and $\zeta \approx 2$, seemingly independently on $\tilde{\mathbf{k}}$. We note that, independently on the normalization choice for ω and k , $H_k \sim k^{1.8}$.

Having established the robustness of the NFH predictions even for nonperfectly 1D systems, as well as the expected universal behavior of the energy correlators for 2D systems, it is interesting to observe what happens if the local conservation of the angular momentum L is violated (i.e., the number of local conservation rules is reduced).

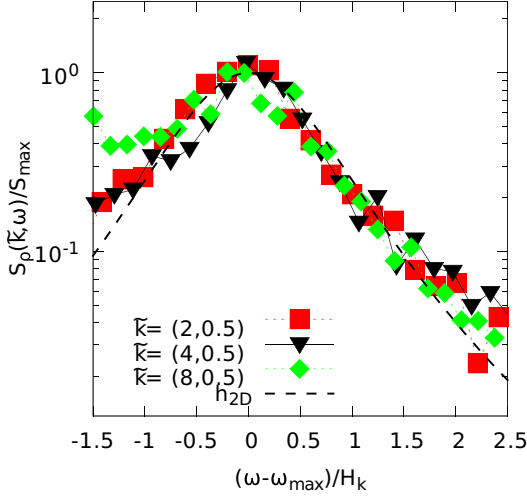


FIG. 7. Data collapse of the rescaled structure factor for a 2D system with $N_c = 256 \times 64$ (points) onto the scaling function h_{2D} given by Eq. (29) (dashed line), for the modes corresponding to $\mathbf{k} = (2, 0.5)$ (squares), $(4, 0.5)$ (downward triangles), and $(8, 0.5)$ (diamonds).

We repeated the numerical experiments described up to now with the same setup, but using the SRD rule to treat the Coulomb collisions. Surprisingly, no evidence of a somewhat different behavior of both S_ρ and C_ε is found, independently on the system size and/or transversal to longitudinal size ratio. As an example, in Fig. 8 we show the energy [Fig. 8(a)] and density current [Fig. 8(b)] correlators as function of ω for the case of quasi-1D system with $N_y = 2$ (i.e., $L_y = L_x/128$) for simulations using DR and SRD protocols (i.e., with and without local conservation of L). The curves do not differ significantly bearing the same $\omega^{-1/3}$ slope at low frequency. In the small inset we also show the density structure factor for $\mathbf{k} = (2, 0.5)$. Also for this quantity no appreciable difference is found, with the sound peak nonappearing to change its position and height, thus implying the persistence of the data collapse to the KPZ scaling function h_{KPZ} [cf. Fig. 6(a)].

C. Effect of the self-consistent \mathbf{E}

It remains to determine the effect of the fluctuations of a globally null electrostatic field on the hydrodynamics of 2D and quasi-1D OCP. We have performed a set of numerical simulations by adding the self-consistent electrostatic field \mathbf{E} , while maintaining the same values for all the other physical parameters.

As anticipated in Sec. III for the typical system sizes considered here the fluctuations $\delta\mathbf{E}$ are of the order of 10^{-6} . In Fig. 9 we show the energy current correlator for the same 2D systems of Fig. 2. We observe that only small systems (i.e., $N_c \leq 32^2$) are significantly affected by the presence of the fluctuating electric field. In particular, it corresponds to the presence of a noisy-like spectrum, i.e., $C_\varepsilon(\omega) \sim \omega^{-2}$, for $\omega < \Omega_p$, showing that the incoherent fluctuations of \mathbf{E} are typically slower than the period associated to the fundamental plasma frequency. This confirms that the fluctuating self-consistent

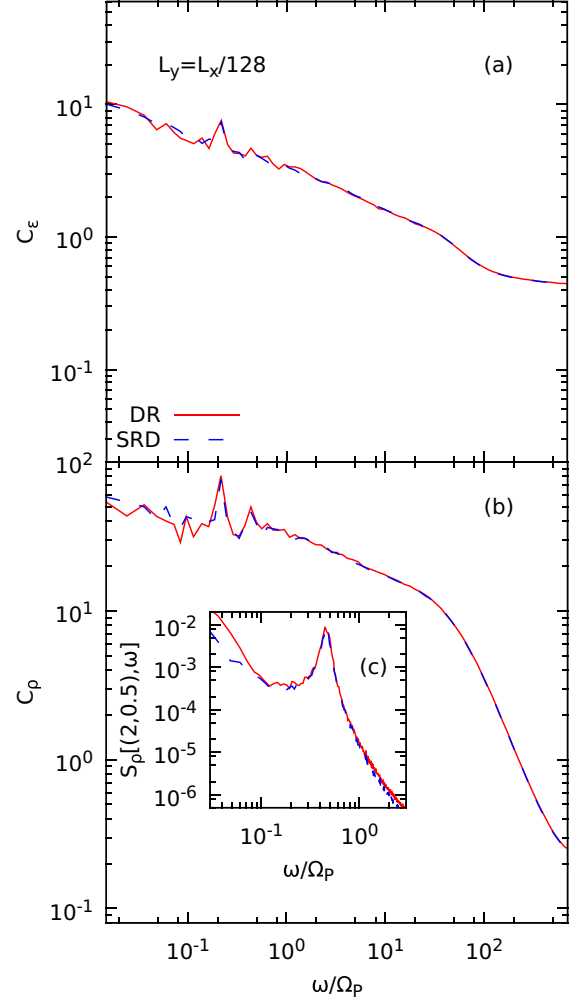


FIG. 8. Fourier spectra of the energy current C_ε , panel (a), and of the density current C_ρ , panel (b), for $\Gamma = 3$, $N_c = 256 \times 2$. The solid lines refer to simulations done with angular momentum conserving DR scheme, while the dashed lines refer to simulations using the standard SRD. The small inset [panel (c)] shows the dynamical structure factor of the density for $\mathbf{k} = (2, 0.5)$. Note how the position and height of the sound peak is not altered.

electric field does not affect the collective behavior of large enough systems.

We have also checked (data not reported) that the crossover from the $\omega^{-1/3}$ power-law divergence to the $\alpha - \beta \log(\omega)$ one, observed for $C_\varepsilon(\omega)$ when passing from 2D to quasi-1D systems, is unaffected by the presence of \mathbf{E} .

Also the relevant features of the density structure factor $S_\rho(\mathbf{k}, \omega)$ do not change with the presence of \mathbf{E} . In Fig. 10 we show this quantity for three values of the normalized wave vector $\mathbf{k} = (2, 0)$, $(4, 0)$, and $(8, 0)$, comparing the results of simulations with the zero-field case: we observe deviations only for small values of ω/Ω_p . In summary, all the results discussed here and at the end of subsection B point out that the hydrodynamics of (quasi)-1D systems is robust with respect to the addition of the angular momentum conservation law as well as to the presence of a “symmetry breaking” mechanism associated to the self-consistent fluctuating electric field.

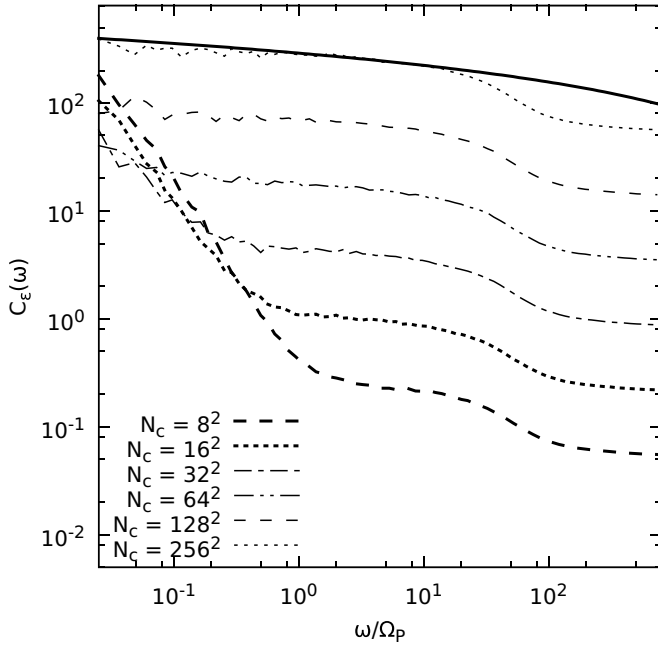


FIG. 9. Fourier spectra C_E of the energy current, for systems with active self consistent \mathbf{E} , $\Gamma = 3$, and $N_c = 8^2, 16^2, 32^2, 64^2, 128^2$, and 256^2 (dashed lines). To guide the eye, the fitting function $f(\omega) \propto \alpha - \beta \log(\omega)$ is added to the figure (heavy solid line).

V. SUMMARY AND CONCLUSIONS

In this paper we have investigated the dynamical structure factors of density and the energy correlators of the one-component plasma model over a few decades in the coupling parameter Γ . The main results are listed hereafter.

When moving from a quasi-one-dimensional setup to a two-dimensional one, we observe a crossover of $C_E(\omega)$ from a power law to a logarithmic divergence at small values of ω . Such a hydrodynamic behavior indicates that the thermal

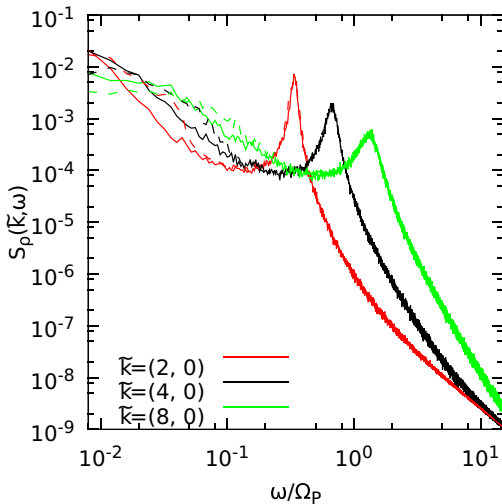


FIG. 10. Dynamical structure factor of density for a quasi-1D system with $L_y = L_x/128$ and $\Gamma = 3$, for $\mathbf{k} = (2,0), (4,0)$, and $(8,0)$. Dashed lines refer to the simulations with activated \mathbf{E} , while the solid lines to those with \mathbf{E} set to 0.

conductivity κ diverges with the system size as $\kappa \sim N^{1/3}$ for 1D systems and as $\kappa \sim \log N$ for 2D systems.

This picture is confirmed also by the form of the structure factors $S_\rho(\mathbf{k}, \omega)$ that are fitted by the KPZ scaling function for quasi-1D systems and by a suitable rational function Eq. (29) for 2D systems.

This numerical result seems to suggest that also in the 2D case a scaling function exists, which should stem from a suitable hydrodynamic theory. Working out such a theoretical approach to the hydrodynamics of 2D OCP goes beyond the aims of this paper and will be open to future investigations.

When the angular momentum conservation law is removed, we do not observe any significant change of the previous results, apart the presence of finite-size effects for small values of ω . This indicates that modes associated with angular momentum conservation have no practical influence on the hydrodynamics of the model in 1D as well as in 2D systems.

The addition of a self-consistent electrostatic field \mathbf{E} to the plasma dynamics also reveals immaterial to the hydrodynamic properties of the model, at least for small amplitude fluctuations of the field. In fact, in the explored parameter space the average value of \mathbf{E} vanishes (neutral plasma), while the amplitude of its fluctuations σ_E is typically of $O(10^{-6})$ and further decreases with the system size. We cannot exclude that for larger amplitudes the overall scenario might change significantly. In addition, we point out that, substituting \mathbf{E} with an opportunely tuned zero-average stochastic field \mathbf{E}_s , with fluctuations with amplitude of the same order of σ_E , will not lead to the same conclusions. The reason of this being that when \mathbf{E} is evaluated self-consistently the dynamics of charge density fluctuations $\delta\rho$ and field fluctuations $\delta\mathbf{E}$ are linked by Maxwell equations, while on the other hand, density fluctuations obviously can not have any effect on an externally imposed field.

The natural follow-up of this work is the extension of our investigation to the case of three dimensional systems where a source of anisotropy is introduced, such as, for instance, an axial magnetic field \mathbf{B}_z is turned on. In this case energy transport is expected to work differently along and perpendicularly to the direction of \mathbf{B}_z . Moreover, as mentioned previously, hybrid MPC-PIC schemes seem to be promising for the modelization of plasma regimes in which the interplay between collisions and macroscopic electromagnetic fields is strong, such as for example the formation of run-away electrons in tokamak plasmas [78,79]. A paper exploring this line is currently in preparation.

ACKNOWLEDGMENTS

We thank V. Popkov, P. Ghendrih, and F. Piazza for the stimulating discussions at an early stage of this project. This work is part of the project CEA-01 “ESKAPE” EUROfusion Enabling Research work programme 2017. G.C. would like to acknowledge the support from A*MIDEX project (Grant No. ANR-11-IDEX-0001-02) funded by the “Investissements d’Avenir” French Government program, managed by the French National Research Agency (ANR). P.F.D.C. acknowledges the support by the INFN initiative DYNYSMATH 2016.

**APPENDIX: LOCAL CONSERVATION RULES
IN SRD AND DR**

We prove here the local conservation rules in SRD and DR schemes. For reasons of simplicity we set particle masses $m = 1$ so that in Eq. (16) $M_i = N_i$.

$$\sum_{j=1}^{N_i} (\mathbf{u}_i + \hat{\mathbf{R}}_i \mathbf{v}_j - \hat{\mathbf{R}}_i \mathbf{u}_i) = N_i \mathbf{u}_i + \hat{\mathbf{R}}_i \sum_{j=1}^{N_i} \mathbf{v}_j - \hat{\mathbf{R}}_i N_i \mathbf{u}_i = \sum_{j=1}^{N_i} \mathbf{v}_j + \hat{\mathbf{R}}_i N_i \sum_{j=1}^{N_i} \mathbf{v}_j - \hat{\mathbf{R}}_i N_i \sum_{j=1}^{N_i} \mathbf{v}_j = \sum_{j=1}^{N_i} \mathbf{v}_j, \quad (\text{A1})$$

which proves the equality.

The conservation of (twice) the kinetic energy $2K_i$ proceeds in the same fashion by substituting the definition of \mathbf{v}'_j in Eq. (19), so that it now reads

$$\begin{aligned} & \sum_{j=1}^{N_i} (\mathbf{u}_i + \hat{\mathbf{R}}_i \mathbf{v}_j - \hat{\mathbf{R}}_i \mathbf{u}_i) \cdot (\mathbf{u}_i + \hat{\mathbf{R}}_i \mathbf{v}_j - \hat{\mathbf{R}}_i \mathbf{u}_i) \\ &= N_i \mathbf{u}_i^2 + \sum_{j=1}^{N_i} (\hat{\mathbf{R}}_i \mathbf{v}_j)^2 + \sum_{j=1}^{N_i} (\hat{\mathbf{R}}_i \mathbf{u}_i)^2 + 2\mathbf{u}_i \cdot \sum_{j=1}^{N_i} \hat{\mathbf{R}}_i \mathbf{v}_j - \sum_{j=1}^{N_i} 2(\mathbf{u}_i \cdot \hat{\mathbf{R}}_i \mathbf{u}_i) - 2 \sum_{j=1}^{N_i} (\hat{\mathbf{R}}_i \mathbf{v}_j) \cdot \hat{\mathbf{R}}_i \mathbf{u}_i \\ &= 2N_i \mathbf{u}_i^2 + \sum_{j=1}^{N_i} \mathbf{v}_j^2 - 2N_i \hat{\mathbf{R}}_i \mathbf{u}_i \cdot \hat{\mathbf{R}}_i \mathbf{u}_i = 2N_i \mathbf{u}_i^2 + \sum_{j=1}^{N_i} \mathbf{v}_j^2 - 2N_i \mathbf{u}_i^2 = \sum_{j=1}^{N_i} \mathbf{v}_j^2, \end{aligned} \quad (\text{A2})$$

where we have used the relation $\hat{\mathbf{R}}_i \mathbf{u}_i \cdot \hat{\mathbf{R}}_i \mathbf{u}_i = \mathbf{u}_i^2$.

So far, the conservation of momentum and kinetic energy in the cell is verified for every rotation matrix $\hat{\mathbf{R}}$. In order to conserve angular momentum, the DR scheme poses a constraint on the choice of the rotation angle φ_i . Let us assume that the rotation matrix $\hat{\mathbf{R}}_{\varphi_i}$ verifies identity Eq. (23), therefore

$$\begin{aligned} & \sum_{j=1}^{N_i} \mathbf{r}_j \wedge [\mathbf{u}_i - \hat{\mathbf{R}}_{\varphi_i} (\mathbf{v}_j - \mathbf{u}_i)] \\ &= N_i \mathbf{r}_i^c \wedge \mathbf{u}_i + \sum_{j=1}^{N_i} \mathbf{r}_j \wedge \hat{\mathbf{R}}_{\varphi_i} (\mathbf{v}_j - \mathbf{u}_i) \\ &= N_i \mathbf{r}_i^c \wedge \mathbf{u}_i + \sum_{j=1}^{N_i} \mathbf{r}_j \wedge \hat{\mathbf{R}}_{\varphi_i} \mathbf{v}_j^c. \end{aligned} \quad (\text{A3})$$

In the equality above, $\mathbf{r}_i^c = (\sum_j \mathbf{r}_j)/N_i$ is the position of the center of mass of cell i and \mathbf{v}_j^c are particles velocities in the center of mass frame.

Let us now rewrite the last term in Eq. (A3) explicitly as function of the components of \mathbf{v}_j^c and \mathbf{r}_j and the rotation angle φ_i as

$$\begin{aligned} & \sum_{j=1}^{N_i} \mathbf{r}_j \wedge \hat{\mathbf{R}}_{\varphi_i} \mathbf{v}_j^c = \cos \varphi_i \sum_{j=1}^{N_i} (x_j v_{yj}^c - y_j v_{xj}^c) \\ & \quad + \sin \varphi_i \sum_{j=1}^{N_i} (-x_j v_{xj}^c - y_j v_{yj}^c) \\ &= \cos \varphi_i \sum_{j=1}^{N_i} \mathbf{r}_j \wedge \mathbf{v}_j^c - \sin \varphi_i \sum_{j=1}^{N_i} \mathbf{r}_j \cdot \mathbf{v}_j^c. \end{aligned} \quad (\text{A4})$$

In order to check the conservation of linear momentum \mathbf{P}_i within the i th cell under the SRD rule, let us substitute the definition of particles relative velocities Eq. (17) in the right-hand side of Eq. (18). Making use of the definition of cell center of mass velocity $\mathbf{u}_i = (\sum_j \mathbf{v}_j)/N_i$, one has

Therefore, one has

$$\begin{aligned} \sum_{j=1}^{N_i} \mathbf{r}_j \wedge \mathbf{v}_j &= N_i \mathbf{r}_i^c \wedge \mathbf{u}_i + \cos \varphi_i \sum_{j=1}^{N_i} \mathbf{r}_j \wedge \mathbf{v}_j^c \\ & \quad - \sin \varphi_i \sum_{j=1}^{N_i} \mathbf{r}_j \wedge \mathbf{v}_j^c \end{aligned} \quad (\text{A5})$$

and

$$\sum_{j=1}^{N_i} \mathbf{r}_j \wedge (\mathbf{v}_j^c + \mathbf{u}_i) = \sum_{j=1}^{N_i} \mathbf{r}_j \wedge \mathbf{v}_j^c + N_i \mathbf{r}_j \wedge \mathbf{u}_i. \quad (\text{A6})$$

Equating the two expressions above, and collecting the terms in sine and cosine finally leads to

$$(1 - \cos \varphi_i) \sum_{j=1}^{N_i} \mathbf{r}_j \wedge \mathbf{v}_j^c + \sin \varphi_i \sum_{j=1}^{N_i} \mathbf{r}_j \cdot \mathbf{v}_j^c = 0, \quad (\text{A7})$$

which is verified when φ_i is such that the definitions in Eqs. (21) and (22) hold, thus proving the conservation of the cell angular momentum for this choice of the rotation angle φ_i .

Note that the rotation operator allows only to preserve up to three conservation laws, therefore, in order to design an MPC scheme accounting for additional conservation laws (e.g., spin), other suitable operators should be introduced. Note also that, imposing the conservation of angular momentum with a rotation is possible only in two dimensions. However, in a 3D system it is still possible to conserve one of the three components of $\mathbf{L} = (L_x, L_y, L_z)$, say L_z , by imposing z as rotation axis in each cell, and computing φ_i from Eq. (20), where now a_i is the z component of the vector $\mathbf{a}_i = \sum_{j=1}^{N_i} \mathbf{r}_j \times (\mathbf{v}_j - \mathbf{u}_i)$.

- [1] S. Lepri, R. Livi, and A. Politi, *Phys. Rep.* **377**, 1 (2003).
- [2] A. Dhar, *Adv. Phys.* **57**, 457 (2008).
- [3] S. Lepri, *Thermal Transport in Low Dimensions: From Statistical Physics to Nanoscale Heat Transfer*, Vol. 921 (Springer, Berlin, 2016).
- [4] S. Lepri, R. Livi, and A. Politi, *Phys. Rev. Lett.* **78**, 1896 (1997).
- [5] L. Wang, N. Li, and P. Hänggi, in *Thermal Transport in Low Dimensions* (Springer, Berlin, 2016), pp. 239–274.
- [6] A. Lippi and R. Livi, *J. Stat. Phys.* **100**, 1147 (2000).
- [7] L. Wang, B. Hu, and B. Li, *Phys. Rev. E* **86**, 040101 (2012).
- [8] H. van Beijeren, *Phys. Rev. Lett.* **108**, 180601 (2012).
- [9] H. Spohn, *J. Stat. Phys.* **154**, 1191 (2014).
- [10] H. Spohn, in *Thermal Transport in Low Dimensions* (Springer, Berlin, 2016), pp. 107–158.
- [11] M. Kardar, G. Parisi, and Y.-C. Zhang, *Phys. Rev. Lett.* **56**, 889 (1986).
- [12] H. Spohn and G. Stoltz, *J. Stat. Phys.* **160**, 861 (2015).
- [13] Z. Rieder, J. L. Lebowitz, and E. Lieb, *J. Math. Phys.* **8**, 1073 (1967).
- [14] X. Zotos, *J. Low Temp. Phys.* **126**, 1185 (2002).
- [15] V. Popkov, A. Schadschneider, J. Schmidt, and G. M. Schütz, *Proc. Natl. Acad. Sci. U.S.A.* **112**, 12645 (2015).
- [16] P. Grassberger and L. Yang, *arXiv:cond-mat/0204247* (2002).
- [17] A. V. Savin, V. Zolotarevskiy, and O. V. Gendelman, *Europhys. Lett.* **113**, 24003 (2016).
- [18] K. Saito, S. Takesue, and S. Miyashita, *Phys. Rev. E* **59**, 2783 (1999).
- [19] D. Barik, *Eur. Phys. J. B* **56**, 229 (2007).
- [20] L. Delfini, S. Lepri, and R. Livi, *J. Stat. Mech.: Theory Exp.* (2005) P05006.
- [21] M. J. Gillan, *J. Phys. C* **7**, L1 (1974).
- [22] M. Baus and J.-P. Hansen, *Phys. Rep.* **59**, 1 (1980).
- [23] T. C. Killian, T. Pattard, T. Pohl, and J. M. Rost, *Phys. Rep.* **449**, 77 (2007).
- [24] G. Bannasch, J. Castro, P. McQuillen, T. Pohl, and T. C. Killian, *Phys. Rev. Lett.* **109**, 185008 (2012).
- [25] S. Tanaka and S. Ichimaru, *Phys. Rev. A* **35**, 4743 (1987).
- [26] D. H. E. Dubin, *Phys. Rev. A* **42**, 4972 (1990).
- [27] M. Bonitz, P. Ludwig, H. Baumgartner, C. Henning, A. Filinov, D. Block, O. Arp, A. Piel, S. Käding, Y. Ivanov *et al.*, *Phys. Plasmas* **15**, 055704 (2008).
- [28] S. Ichimaru, H. Iyetomi, S. Mitake, and N. Itoh, *ApJ Lett.* **265**, L83 (1983).
- [29] F. V. de Blasio, *Nuovo Cimento A Serie* **108**, 431 (1995).
- [30] J. Hughto, *J. Phys.: Conf. Ser.* **342**, 012005 (2012).
- [31] D. A. Baiko and D. G. Yakovlev, *Astron. Lett.* **21**, 702 (1995).
- [32] T. Ott, M. Bonitz, and Z. Donkó, *Phys. Rev. E* **92**, 063105 (2015).
- [33] S. Pfalzner, *An Introduction to Inertial Confinement Fusion: Series in Plasma Physics*, Vol. 19 (Taylor & Francis, London, 2006).
- [34] K. Kremer, M. O. Robbins, and G. S. Grest, *Phys. Rev. Lett.* **57**, 2694 (1986).
- [35] E. R. Russell, F. Spaepen, and D. A. Weitz, *Phys. Rev. E* **91**, 032310 (2015).
- [36] Z. Donkó, G. J. Kalman, and P. Hartmann, *J. Phys.: Condens. Matter* **20**, 413101 (2008).
- [37] J. P. Mithen, J. Daligault, B. J. B. Crowley, and G. Gregori, *Phys. Rev. E* **84**, 046401 (2011).
- [38] D. H. Dubin and T. M. O’neil, *Rev. Mod. Phys.* **71**, 87 (1999).
- [39] A. Malevanets and R. Kapral, *J. Chem. Phys.* **110**, 8605 (1999).
- [40] A. Malevanets and R. Kapral, in *Novel Methods in Soft Matter Simulations*, edited by M. Karttunen, A. Lukkarinen, and I. Vattulainen, Vol. 640 of Lecture Notes in Physics (Springer Verlag, Berlin, 2004), pp. 116–149.
- [41] R. Kapral, *Multiparticle Collision Dynamics: Simulation of Complex Systems on Mesoscales* (John Wiley & Sons Inc., New York, 2008), pp. 89–146.
- [42] P. Di Cintio, R. Livi, H. Bufferand, G. Ciraolo, S. Lepri, and M. J. Straka, *Phys. Rev. E* **92**, 062108 (2015).
- [43] T. Ott, Z. Donkó, and M. Bonitz, *Contrib. Plasma Phys.* **56**, 246 (2016).
- [44] J. Struckmeier, *Phys. Rev. Spec. Top.: Accel. Beams* **3**, 034202 (2000).
- [45] H. E. Kandrup, I. V. Sideris, and C. L. Bohn, *Phys. Rev. Spec. Top.: Accel. Beams* **7**, 014202 (2004).
- [46] H. Bufferand, G. Ciraolo, Y. Marandet, J. Bucalossi, P. Ghendrih, J. Gunn, N. Mellet, P. Tamain, R. Leybros, N. Fedorczak *et al.*, *Nucl. Fusion* **55**, 053025 (2015).
- [47] J. Omotani, I. Pusztai, S. Newton, and T. Fülöp, *Nucl. Fusion* **56**, 124002 (2016).
- [48] T. Ott, M. Bonitz, L. G. Stanton, and M. S. Murillo, *Phys. Plasmas* **21**, 113704 (2014).
- [49] T. Ott, M. Stanley, and M. Bonitz, *Phys. Plasmas* **18**, 063701 (2011).
- [50] T. H. Stix, *Waves in Plasmas* (Springer, Berlin, 1992).
- [51] Z. Donkó, J. Goree, P. Hartmann, and B. Liu, *Phys. Rev. E* **79**, 026401 (2009).
- [52] L. Spitzer, *Physics of Fully Ionized Gases* (John Wiley & Sons Inc., New York, 1965).
- [53] I. Korolov, G. J. Kalman, L. Silvestri, and Z. Donkó, *Contrib. Plasma Phys.* **55**, 421 (2015).
- [54] B. Bernu, P. Vieillefosse, and J. P. Hansen, *Phys. Lett. A* **63**, 301 (1977).
- [55] B. Bernu and P. Vieillefosse, *Phys. Rev. A* **18**, 2345 (1978).
- [56] S. Takeno and F. Yoshida, *Prog. Theor. Phys.* **62**, 883 (1979).
- [57] J. W. Eastwood, R. W. Hockney, and D. N. Lawrence, *Comput. Phys. Commun.* **19**, 215 (1980).
- [58] Z. Donkó, G. J. Kalman, P. Hartmann, K. I. Golden, and K. Kutasi, *Phys. Rev. Lett.* **90**, 226804 (2003).
- [59] R. W. Hockney and J. W. Eastwood, *Computer Simulation Using Particles* (Taylor & Francis, London, 1981).
- [60] G. Gompper, T. Ihle, D. M. Kroll, and R. G. Winkler, *Multi-Particle Collision Dynamics: A Particle-Based Mesoscale Simulation Approach to the Hydrodynamics of Complex Fluids* (Springer, Berlin, 2009), p. 1.
- [61] C. M. Pooley and J. M. Yeomans, *J. Phys. Chem. B* **109**, 6505 (2005).
- [62] H. Noguchi and G. Gompper, *Phys. Rev. E* **78**, 016706 (2008).
- [63] M. Yang, M. Theers, J. Hu, G. Gompper, R. G. Winkler, and M. Ripoll, *Phys. Rev. E* **92**, 013301 (2015).
- [64] J. Ryder, Ph.D. thesis, Oxford University, UK, 2005.
- [65] M. Belushkin, R. Livi, and G. Foffi, *Phys. Rev. Lett.* **106**, 210601 (2011).
- [66] T. Ihle and D. M. Kroll, *Phys. Rev. E* **63**, 020201 (2001).
- [67] T. Ihle and D. M. Kroll, *Phys. Rev. E* **67**, 066705 (2003).
- [68] H. Bufferand, G. Ciraolo, P. Ghendrih, P. Tamain, F. Bagnoli, S. Lepri, and R. Livi, *J. Phys.: Conf. Ser.* **260**, 012005 (2010).
- [69] H. Bufferand, G. Ciraolo, P. Ghendrih, S. Lepri, and R. Livi, *Phys. Rev. E* **87**, 023102 (2013).

- [70] O. D. Kellogg, *Foundations of Potential Theory* (Springer, Berlin, 1967), p. 1.
- [71] M. Fellhauer, P. Kroupa, H. Baumgardt, R. Bien, C. M. Boily, R. Spurzem, and N. Wassmer, *New Astron.* **5**, 305 (2000).
- [72] M. Frigo and S. G. Johnson, FFTW: Fastest Fourier Transform in the West, Astrophysics Source Code Library (2012).
- [73] W. H. Press, S. A. Teukolsky, W. T. Vetterling, and B. P. Flannery, *Numerical Recipes in C++ : The Art of Scientific Computing* (Cambridge University Press, Cambridge, UK, 2002).
- [74] P. Di Cintio, Ph.D. thesis, Technische Universität Dresden, 2014.
- [75] H. Grubmüller, H. Heller, A. Windemuth, and K. Schulten, *Mol. Simul.* **6**, 121 (1991).
- [76] L. Casetti, *Phys. Scr.* **51**, 29 (1995).
- [77] M. Prähofer and H. Spohn, *J. Stat. Phys.* **115**, 255 (2004).
- [78] A. Stahl, O. Embréus, M. Landreman, G. Papp, and T. Fülöp, *J. Phys. Conf. Series* **775**, 012013 (2016).
- [79] A. Stahl, O. Embréus, G. Papp, M. Landreman, and T. Fülöp, *Nucl. Fusion* **56**, 112009 (2016).